A RADIATOR CONCEPT BASED ON CAPILLARY RETENTION OF LIQUID

by Alex Vary

Lewis Research Center
Cleveland, Ohio

A RADIATOR CONCEPT BASED ON CAPILLARY RETENTION OF LIQUID

By Alex Vary

Lewis Research Center
Cleveland, Ohio

NATIONAL AERONAUTICS AND SPACE ADMINISTRATION

ABSTRACT

A preliminary study was made to define problem areas and potential advantages of a radiator for extraterrestrial applications in which a heat exchange liquid is circulated through a capillary medium. An evaluation of surface energy, heat transfer, hydraulic, geometric, and meteoroid penetration factors in a capillary radiator operating under extraterrestrial conditions is presented to indicate feasibility in a potential application.

STAR Category 03

CONTENTS

A RADIATOR CONCEPT BASED ON CAPILLARY RETENTION OF LIQUID

by Alex Vary

Lewis Research Center

SUMMARY

A radiator concept in which a heat exchange liquid is circulated in a capillary me-
dium contained in heat radiating panels is described. It is proposed that this concept
may be applied to space systems where the possibility of meteoroid punctures exists.
An argument based on well-known surface energy phenomena is presented to show that
capillary retention of liquid at puncture sites can be expected to halt liquid leakage under
certain conditions. Liquid escape by the alternative mode of vaporization can be sub-
stantially reduced by employing liquids having low vapor pressures and by operating the
radiator at sufficiently low temperatures.

The feasibility of a radiator based on the capillary concept operating under extrater-
restrial conditions is examined in terms of surface energy, heat transfer, fluid dynamic,
geometric, and meteoroid penetration factors. Estimates of the significant character-
istics of a hypothetical capillary radiator indicate that the concept is potentially com-
petitive with other concepts being considered for space application. However, a firm
conclusion concerning feasibility must be deferred until there is experimental evidence
of the viability of liquid-filled capillary media subjected to the conditions of an actual
space application. Problems associated with the concept are defined, and resolutive
investigations are suggested.

Because of the preliminary nature of this study, predictions of the potential advan-
tages of using a capillary radiator are speculative. Nevertheless, some possible advan-
tages include lower specific weight, lower temperature, higher power cycle efficiency,
and less restriction on the radiator size relative to the conventional fin-tube concept.

INTRODUCTION

Liquid- or vapor-filled radiators that are being considered for space applications
should incorporate features that provide adequate protection against the deleterious

effects of meteoroid impacts. Present design concepts include the use of armor, "bumper" plates, or reinforced tube walls to reduce vulnerability to meteoroid punctures. In large space powerplants the radiator weight with respect to useful power may be significantly higher than that of any other major component in interplanetary vehicles (ref. 1). Recent efforts in radiator design therefore have been directed toward reducing not only the vulnerability to meteoroid punctures but also the weight penalty arising from meteoroid protection requirements (refs. 2 and 3).

The radiator concept that is currently contemplated for space powerplants is based on the circulation of heat exchange fluid in a fin-and-tube structure protected by reinforcement or armor (refs. 4 and 5). Other radiator concepts that have been proposed are described in references 2, 3, and 6. The concept proposed herein is based on a capillary structure that is inherently vulnerable to meteoroid puncture but relies on capillary retention of the heat exchange liquid at anticipated puncture sites.

In the proposed "capillary radiator" concept, the prime heat radiating surfaces consist of thin panels containing a capillary medium within which the heat exchange liquid circulates. When the panels are damaged by meteoroids, surface energy phenomena should prevent leakage if certain conditions are satisfied. Liquid loss which would then occur by evaporation can be reduced by selecting liquids having low vapor pressures and by operating the radiator at temperatures that produce low vaporization rates.

The purpose of this report is to indicate the feasibility of a liquid-filled, capillary radiator that will experience numerous punctures by meteoroids. Possible advantages and problems associated with a capillary radiator are also discussed.

FUNDAMENTAL CONSIDERATIONS

General Description

The capillary radiator consists of a number of thin extensive panels containing a capillary medium saturated with a heat exchange liquid. The panels are attached to pipes that convey the liquid between the radiator and a heat exchanger by means of a suitable pumping and distribution scheme.

Internally the panels may consist of layers of sheet metal separated by spacers or of foam metal sandwiched between surface layers of sheet metal, as illustrated in figure 1. There are many other equivalent modes of capillary construction; for example, laminations of corrugated sheet metal, laminations of wire mesh screens, metal fiber wicks, metallic sponges, and so forth. The crucial feature of a suitable capillary medium would be an intercommunicating cellular substructure. This "connected" cell feature is necessary to provide flow channels around discontinuities and obstructions that arise from meteoroid impacts.
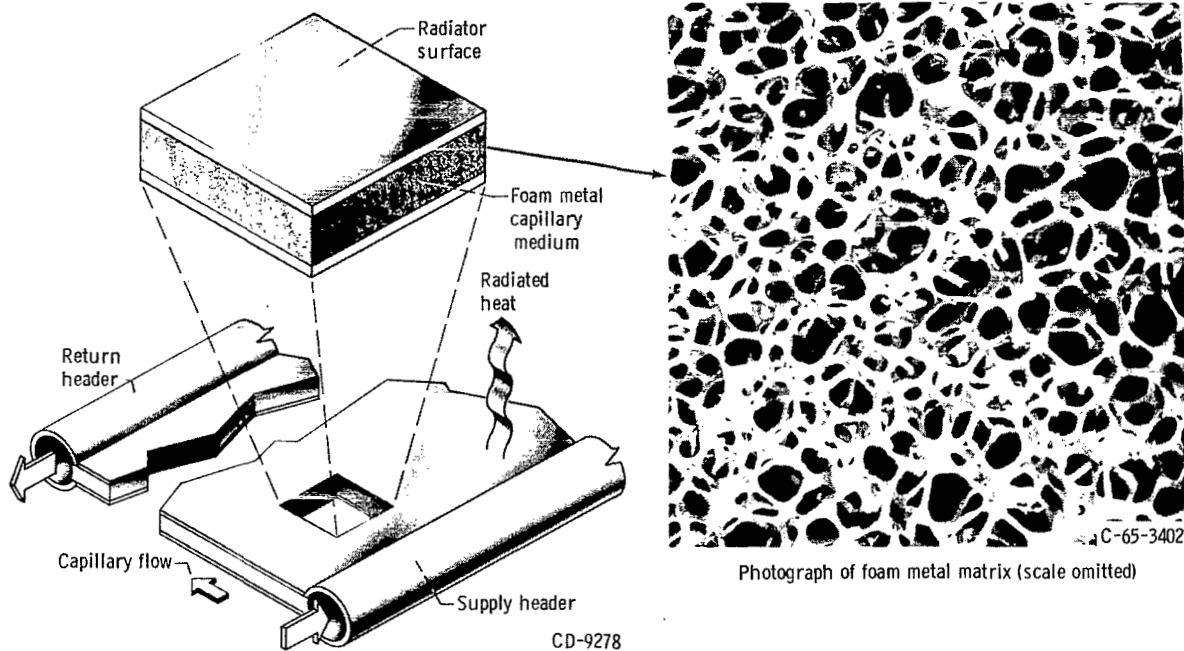
Figure 1. - Segment of typical capillary radiator.

Photograph of foam metal matrix (scale omitted)

C-65-3402

CD-9278

Analysis of Capillary Retention

The purpose of this section is to identify surface energy factors that influence capillary retention of liquid flowing past punctures in a capillary medium. It will be shown that the design of a capillary radiator depends on the specification of a capillary dimension and the imposition of certain conditions on the capillary medium and circulatory system.

Basic phenomena and prerequisite conditions. - To obtain a general expression for specifying the capillary dimension, it is necessary to consider the surface tension effects that are discussed hereinafter.

Throughout the following discussion, it is assumed that the equilibrium contact angle lies between 0° and 180°. A crucial factor to the capillary radiator concept is the prerequisite condition that the cohesive forces in the liquid be greater than the adhesive forces with respect to the container material (i. e. , no spontaneous spreading). The following discussion pertains to a zero- or low-gravity vacuum environment.

Figure 2 shows a cross section of the liquid near the end of a cylindrical capillary tube with diameter δ_e. The illustration represents a "clean break" or right truncation of one element of a radiator consisting of an array of tubular channels. Under zero
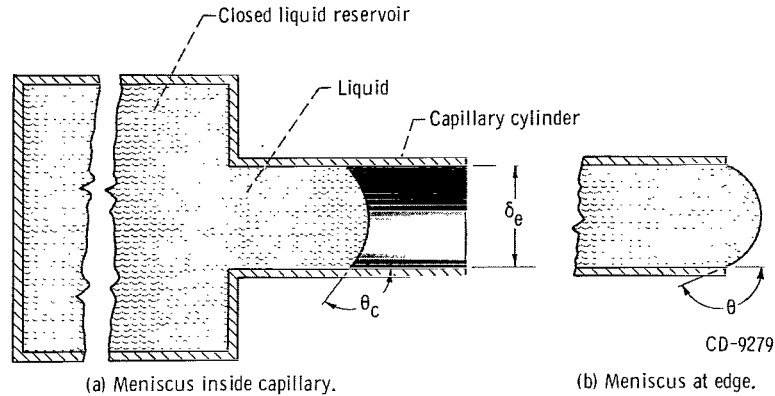
Figure 2. - Cross section of liquid-filled capillary tube in zero gravity.

gravity, the curvature of the meniscus depends solely on surface tension forces.

If the liquid is nonwetting, a convex meniscus as depicted in figure 2(a) will form upon exposure of the liquid surface and the contact angle will be greater than 90°. If the liquid surface is displaced (as, for example, by increasing the liquid inventory) so that the meniscus is at the lip of the tube (fig. 2(b)), then surface tension effects restrain the liquid from climbing over the edge of the tube. This restraint exists as long as the angle at the edge θ does not exceed the contact angle θ_c increased by 90°. A familiar example of the "edge effect" (see ref. 7) is the surface tension phenomenon that allows overfilling of a tumbler of water. A discontinuity such as an edge will bar movement of a liquid surface and allow the meniscus curvature to change with the liquid pressure.

The angle θ is measured between the surface and tangent to the meniscus at the edge as indicated in figure 2(b); θ is equal to or greater than θ_c the equilibrium contact angle. Although the contact angle is an invariant depending on degree of wetting (ref. 8), the edge angle θ in figure 2(b) can be varied by varying the liquid inventory or pressure. The maximum value of θ is $\theta_c + 90^\circ$ as noted in the previous paragraph.

A "contact angle hysteresis" (refs. 7 and 8) occurs with wetting as well as non-wetting liquids whenever an interface tends to move. Because of the edge and hysteresis effects, the liquid pressure may be different from the equilibrium pressure established by the usual contact angle. The surfaces and edges needed to exploit these effects are assumed to exist in the capillary matrix.

The previously described phenomena may be applied to liquid retention at meteoroid puncture sites in a capillary medium. For example, when a puncture occurs and a quantity of liquid is lost, if this quantity is not replaced, the liquid surface will reside more or less within the capillary. Then, as in the case illustrated in figure 2(b), a stable meniscus will form for a range of pressures provided that suitable surfaces and edges

4

are available. The edge and hysteresis effects will tend to bar further liquid egress after the initial liquid loss in the absence of large pressure changes.

The pressure that can be supported within the liquid by surface tension forces depends upon the capillary dimension. For a tube with the meniscus at the edge as in figure 2(b), the capillary diameter for which the force of surface tension balances the force of liquid pressure is given by the following equation:

$$P = \frac{4\sigma}{\delta_e} (-\cos \theta) \tag{1}$$

where δ_e is the equilibrium diameter associated with the surface tension σ, pressure P of the liquid, and the variable angle θ. (Symbols are defined in appendix A.) Equation (1) applies only to cases where θ is greater than or equal to the equilibrium contact angle (i.e., $\theta_c \leq \theta \leq \theta_c + 90^\circ$). The external pressure is assumed zero throughout this discussion.

Given δ_e, σ, and $-\cos \theta$, equation (1) sets the maximum pressure at any puncture. Note that P may be zero or negative as when the break meniscus curvature is concave. Note also that for circular tubes as in figure 2(b) the maximum positive pressure occurs when the meniscus is a convex hemisphere. For either wetting or nonwetting liquids, θ will be between 0° and 180°.

(a) Puncture with $d > \delta'_e$.

(b) Puncture with $d < \delta'_e$.
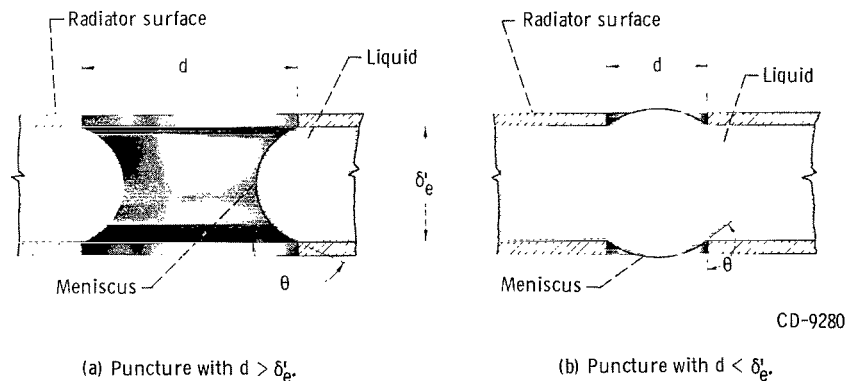
Figure 3. - Hypothetical circular puncture in capillary radiator consisting of two parallel plates.

Selection of the capillary structure. - It is instructive to consider menisci which may arise at hypothetical puncture sites not having circular tubular openings. Consider, for example, an elemental radiator formed of two closely spaced parallel plates with spacing δ'_e and containing liquid at pressure P. In figure 3 a cross section of a right-circular hole with diameter d is shown under conditions where the interface is at the

break edge. If d is greater than δ'_e, the meniscus will be as shown in figure 3(a). For equilibrium δ'_e is determined in accordance with the following equation:

$$\delta'_e = \frac{2\sigma}{P} (-\cos \theta) \qquad (2)$$

In general, for circular holes having $d > \delta'_e$ as in figure 3(a) the critical dimension is δ'_e, the spacing between plates. Figure 3(b) represents the alternative case where $d < \delta'_e$ and the "cylindrical" meniscus of figure 3(a) merges to form two "circular" menisci. For holes having $d < \delta'_e$ as in figure 3(b), the critical dimension is d, the diameter of the hole. Should the hole diameters d invariably be less than δ_e as defined by equation (1) which is applicable to figure 3(b), then the radiator could consist of parallel plates having any convenient spacing. Because punctures with $d > \delta_e$ will invariably occur, δ'_e is bound to be the critical dimension in general.

Unlike the previous idealized case the perimeters of actual punctures will usually be noncircular and nonplanar. For example, consider an elemental radiator formed of two parallel plates having an irregularly shaped hole in the form of a right parallelepiped as illustrated in figure 4. The hole "diameter" exceeds the plate spacing δ' in this case.
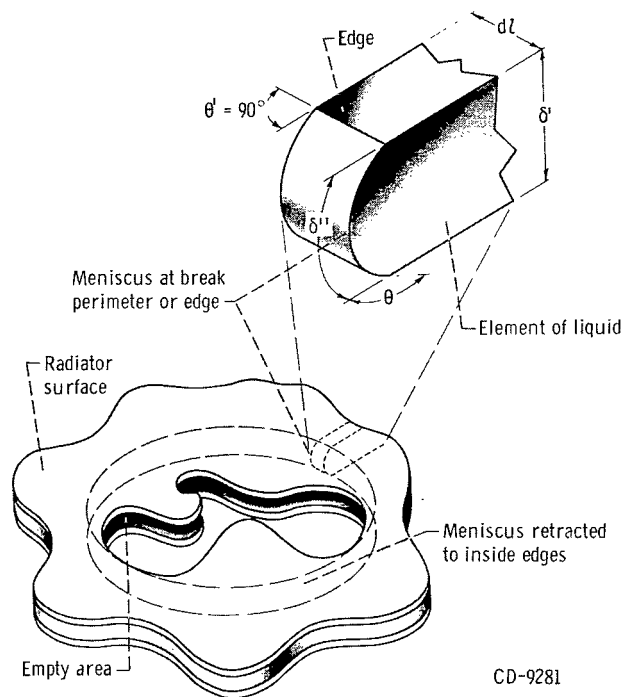

Figure 4. - Irregular puncture in capillary radiator consisting of two parallel plates.

Because of impact distortion, the plate spacing near holes will not be uniform, and generally the meniscus perimeter will be nonplanar. At an edge the force balance for a typical differential element of the meniscus (see fig. 4) with dimensions dl and δ'' will vary with δ', the local plate spacing; so that,

$$P\delta' \, dl = 2\sigma(-\cos\theta) \, dl + 2\sigma(-\cos\theta')\delta''$$

Because the angle θ' relative to contiguous elements of the meniscus is 90°, as indicated in figure 4, the previous equation reduces to equation (2). The minor dimension of noncircular nonplanar menisci should therefore be one-half of δ_e as given by equation (1) for the same pressure P.

In the case of an irregular hole δ'_e as given by equation (2) will generally apply. Temporarily, portions of the meniscus at the edge may be oblique with the critical minor dimension exceeding δ'_e. Consequently, the angle at the edge may be excessive and liquid escape will occur until the meniscus has retracted slightly into the capillary and acquired a critical minor dimension more nearly equal to or less than δ'_e.

For a capillary radiator consisting of a panel of stacked parallel layers of uniformly spaced plates, equation (2) applies with the plate spacing δ as the critical dimension. However, this type of capillary would have serious limitations unless internal edges were provided for liquid interface attachment. Suitable capillary structures would have further partitioning of the space between plates, or a cellular matrix included between the plates. Such a structure, in addition to being mechanically sounder, should enhance capillary retention by introducing additional surfaces and edges to which liquid may adhere. A wick- or sponge-like structure, such as a foam metal matrix with interconnecting pores, would be appropriate. This type of matrix, sandwiched between layers of sheet metal, should be homogeneous with characteristic "pore diameters" that lie within close bounds. Alternatively, the capillary medium may consist of parallel circular tube segments in which case the tube diameter δ_e is related to surface tension and pressure through equation (1).

System interaction factors. - The capillary phenomena upon which the radiator concept is based cannot be considered apart from the total system. Factors that influence capillary retention in a radiator loop under flow conditions become apparent by reference to the system depicted schematically in figure 5. The entire radiator loop, including all noncapillary volumes such as the pump, heat exchanger, and headers, is liquid-filled to capacity. In figure 5 a puncture is shown as a clean break in a cylindrical capillary tube that represents one of the numerous flow channels within the radiator panel. Because the channels are interconnected, alternative flow passages invariably exist around each break as indicated. The radiator flow area may be taken as being very large compared to the area lost because of punctures.
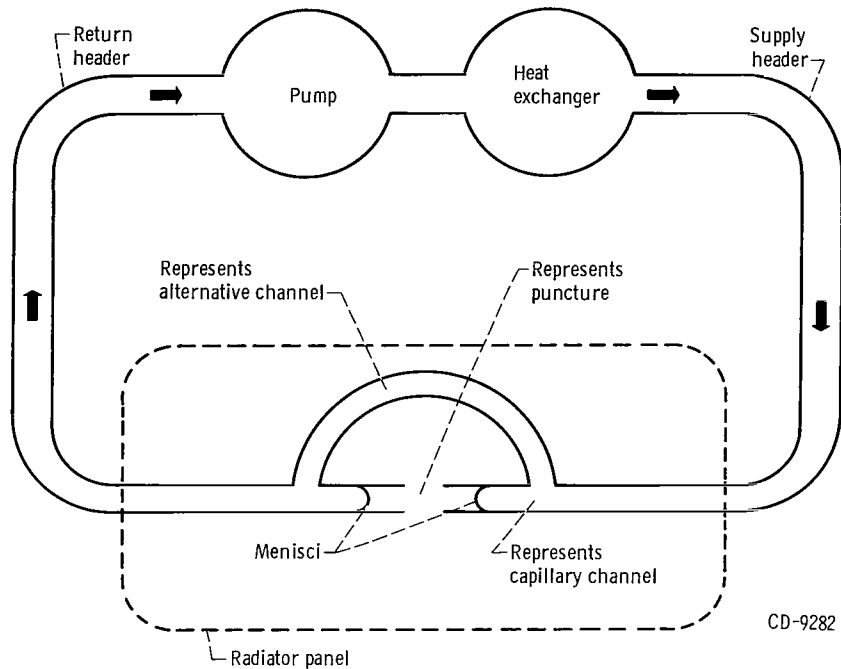
Figure 5. - Schematic of all-liquid radiator loop with break in capillary channel.

When a puncture occurs, a quantity of liquid is expelled along with a quantity of radiator material. If the lost liquid is not replenished, the resultant liquid interface will form within the capillary as in a sponge that is partially emptied by squeezing. Accordingly, menisci that form at the break site will be more or less displaced into the capillary channels. The menisci in figure 5 are both shown convex corresponding to an internal edge angle θ greater than 90° and positive pressure.

Given the aforementioned conditions, in order for liquid to escape, the menisci in figure 5 must move to the lip of the tube and the angle θ must exceed a critical value greater than 90° at the lip to overcome the edge effect. Also, liquid must be withdrawn from elsewhere in the radiator since the amount of liquid is assumed to be constant. If a previous hole exists elsewhere, then the meniscus there must retract to supply the liquid. If the previous menisci have assumed curvatures that agree with the local pressures, no displacement can occur. If there are no previous holes, or if previous menisci are stable, then new menisci must form by a process that does not draw upon liquid from other parts of the system (unless additional liquid is supplied from a separate reservoir.) The capillary structure should be such that menisci can form at punctures sites with curvatures that agree with local pressures established prior to the puncture.

Pressure rise in the radiator pump and absolute pressure levels in the radiator can be tailored to prevent potential leakage from punctures. Figure 6 presents a theoretical
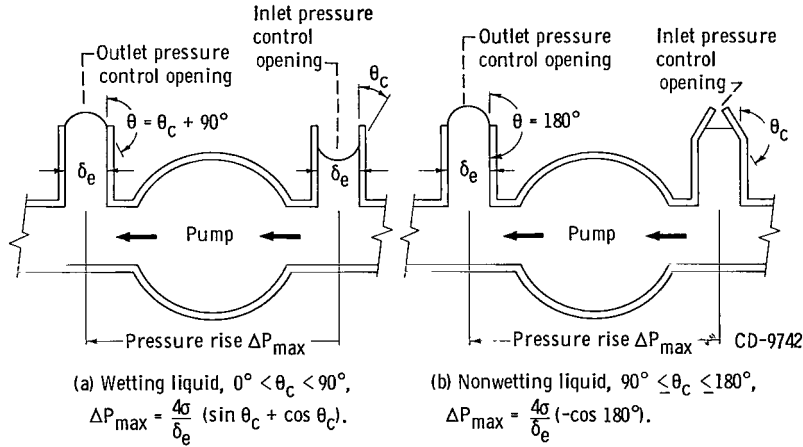
Figure 6. – Scheme for establishing absolute pressure and pressure rise across radiator pump.

scheme for establishing the allowable pressure rise in the pump. In this example, hypothetical "pressure control openings" are located near the pump inlet and outlet. When the pump is operating, the inlet and outlet menisci are displaced as indicated. Provided the maximum allowable pressure rise ΔP_{max} is not exceeded, the menisci will be stationary.

If the liquid wets (fig. 6(a)), then the maximum pressure at the outlet would be $(4\sigma/\delta_e)\left[-\cos(\theta_c + 90°)\right]$ and the minimum pressure at the inlet would be $(4\sigma/\delta_e)(-\cos \theta_c)$. Recall that $\theta_c + 90°$ equals θ maximum. (The openings are cylindrical tubes with diameter δ_e and the external pressure is zero.) This gives a maximum pressure rise of

$$\Delta P_{max} = \frac{4\sigma}{\delta_e} (\sin \theta_c + \cos \theta_c) \tag{3}$$

Note that $1 \le (\sin \theta_c + \cos \theta_c) \le 1.414$ for $0° \le \theta_c \le 90°$.

If the liquid is nonwetting, then the inlet pressure control opening (fig. 6(b)) might, for example, be conical with a slope angle equal to θ_c so that the inlet equilibrium meniscus is flat and the corresponding liquid pressure is zero. At the outlet opening θ may not exceed $180°$ because the liquid pressure is maximum when $\theta = 180°$. For nonwetting liquids the maximum pressure rise may be at least $4\sigma/\delta_e$ for all θ_c. These cases are included to illustrate how the lowest pressure can always be made to assume values such that the allowable pressure rise ΔP_{max} is at least $4\sigma/\delta_e$ for all contact angles θ_c.

Equation (1) can be used to set the maximum pump or radiator pressure. Also, according to the examples given, $-\cos \theta$ in equation (1) may be set equal to 1 to get a

conservative estimate of ΔP_{max} where $\Delta P_{max} = P$. Once the maximum pressure is specified by means of equation (1), a suitable minimum pressure can be obtained.

Equation (3) exemplifies a case where ΔP_{max} can equal or exceed $4\sigma/\delta_e$, but reference 8 suggests that there might be practical limitations on stability when ΔP_{max} exceeds $4\sigma/\delta_e$.

The pressure profile of the radiator system established according to the previous hypothetical scheme should remain unaltered when the radiator is punctured. As explained previously, this can be assured if the capillary matrix has a substructure that provides a suitable array of surfaces and edges.

Liquid drainage at puncture sites in the radiator would tend to occur if noncapillary components such as the pump, headers, or heat exchanger were partially voided and subjected to a sufficiently high pressure. The absence of such voids is therefore a prerequisite. When filled to capacity, systems similar to that shown schematically in figure 5 will retain liquid because of cohesive forces in the liquid in accordance with the previous argument.

If capillary pumping is used, a vapor void is an integral part of the pump. Capillary pumping depends in part on vaporization and condensation for fluid transfer. In this case vapor-liquid interfaces arise in the capillary matrix within the pump. A radiator loop with a low pressure vapor void of this type is capable of holding liquid because of inherent capillary retention within the pump as well as at puncture sites.

The effects of inertial pressures that arise from vehicle accelerations and pulse pressures that accompany high velocity impacts would engender liquid escape if large pressure fluctuations result. Although inertial pressures can be taken into account by design, it is difficult to assess the effect of pulse pressures without experimental data.

Heat Transfer and Fluid Dynamic Considerations

Parametric equations relating heat transfer, hydraulics, fluid properties, and radiator geometry are derived for a hypothetical capillary radiator in the following sections. The purpose of these sections is to evolve analytic expressions by means of which the concept may be evaluated. The evaluation is based on the possibility of selecting a capillary dimension consistent with liquid retention at meteoroid impact sites under the constraints imposed by heat transfer requirements.

Identification of conditional parameters. - In the ensuing discussion the radiator consists of a number n_p of identical thin, flat heat radiating panels. The panels are joined to a central header system and are so disposed with respect to one another as to form the dihedral angle ω as depicted in figure 7. The total radiating area equals $2LWn_p$ where L is the length and W is the width of each panel. Edge radiation is

10
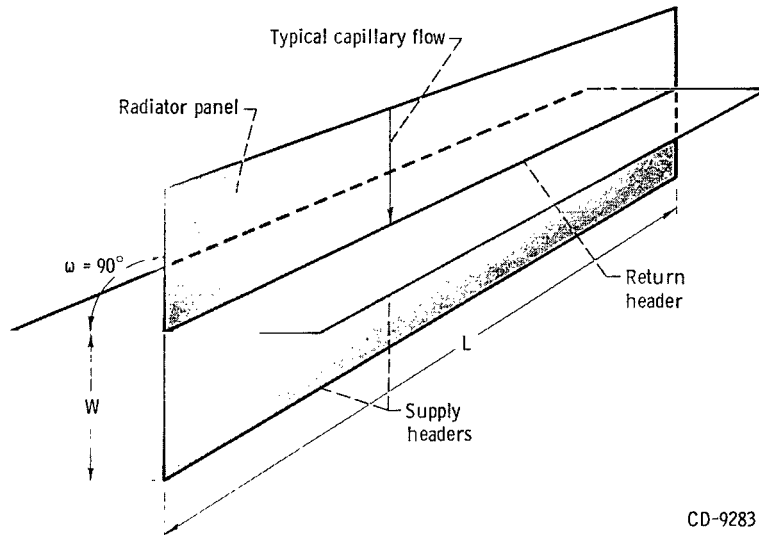
Figure 7. - Capillary radiator with eight radiating surfaces.

ignored because of the small area involved. Given Q, the amount of heat to be rejected, the required radiator area is

$$2LWn_p = \frac{Q}{q} \qquad (4)$$

The radiative heat flux q is a function of the surface emittance, temperature, and dihedral angle between panels (the space environment being regarded as a perfect heat sink); that is,

$$q = f_\omega \epsilon \sigma_B T_s^4 \qquad (5)$$

In the present case the emittance ϵ and T_s, the radiator surface temperature, are assumed to be constant over the radiator surface. The "configuration factor" f_ω assumes values that vary with the dihedral angle ω. An equation relating f_ω to ω is derived in appendix B.

The flow in the panels is shown in figure 8. The radiator panels consist of alternating layers of fluid and metal as depicted in figure 9. Each fluid layer is further partitioned into parallel capillary channels extending across the length of the panels. In each panel the capillary channels accept fluid from a common supply header and empty into a common return header (fig. 8). Header arrangement and size do not enter explicitly into the analysis that follows. The channels are square tubes and have a "nominal diameter" equal to δ.

11
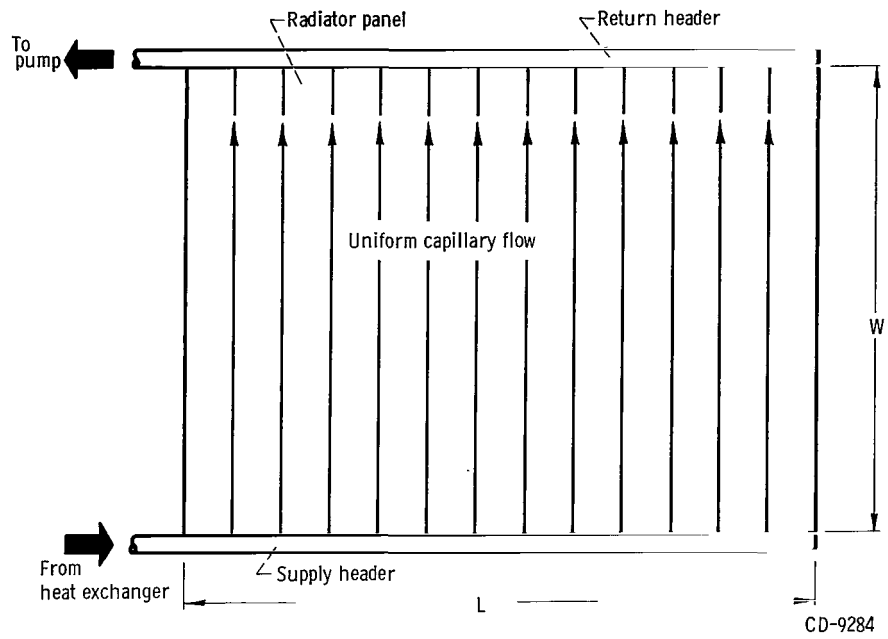
Figure 8. - Schematic of flow scheme in radiator panels.
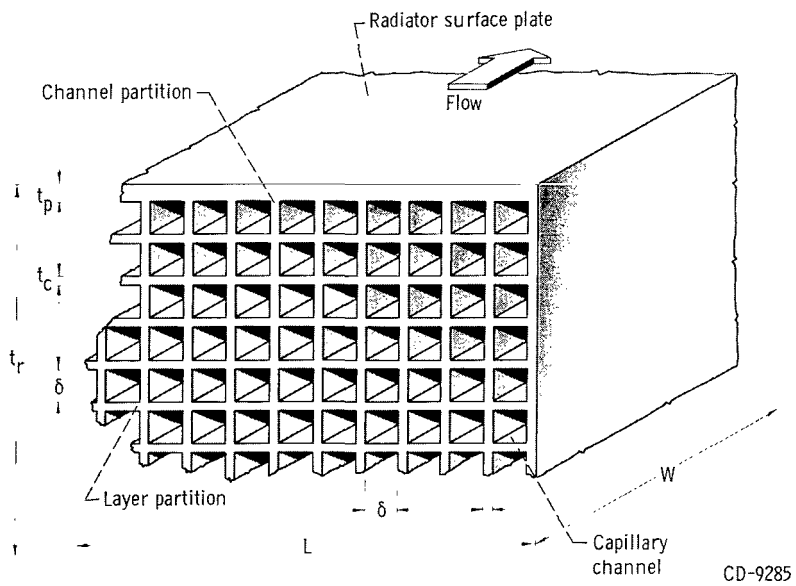
Figure 9. - Representative capillary medium contained within radiator panels.

12

There are n_l layers of channels which, combined with $(n_l + 1)$ alternate layers of surface and partition material, make up the radiator panel thickness in accordance with the following equation:

$$t_r = n_l \delta + (n_l - 1)t_c + 2t_p \tag{6}$$

Note that the radiator surface plates and partitions are not necessarily identical in thickness, $t_p \geq t_c$. The quantity $n_l \delta$ is termed total fluid layer thickness t_l; that is,

$$t_l = n_l \delta \tag{7}$$

There are n_c parallel channels in each layer so that the length L is given by the equation

$$L = n_c \delta + (n_c + 1)t_c \cong n_c(\delta + t_c) \tag{8}$$

The approximate expression is used herein since n_c is considerably greater than one.

Heat transfer and flow relations. - Conductive heat transfer within the radiator delivers heat to the radiator surface at a rate equal to q as is indicated by the following equation:

$$q = \frac{2k(T_i - T_s)}{t_r} \tag{9}$$

In equation (9) k is an average value representing the combined thermal conductivities of the containment structure and fluid, and T_i is the maximum internal temperature.

The mass flow rate in each panel M is

$$M = \frac{Q}{n_p c \, \Delta T} \tag{10}$$

where ΔT is the temperature difference between the radiator inlet and outlet. The mass flow rate is also given by equation (11)

$$M = \rho v n_c n_l \delta^2 \tag{11}$$

The flow velocity v is obtained by the Hagen-Poisseuille equation for laminar flow in circular tubes which is applicable in this case; this equation is

13

$$\Delta P = \frac{32\eta W v}{\delta^2} \tag{12}$$

Arbitrarily setting ΔP equal to $\frac{1}{2}P$ and solving for v yield equation (13). (This procedure assumes that a pressure of $\frac{1}{2}P$ is sufficient to overcome the head loss in the return header.)

$$v = \frac{P\delta^2}{64\eta W} \tag{13}$$

General parametric equation. - Setting δ equal to δ_e, using equation (1) for this case, combining equations (1), (4), (8), (10), (11), and (13), and solving for L in terms of δ yield the following parametric equation:

$$L = \left[\Phi\psi \left(\frac{1 + \dfrac{t_c}{\delta}}{\delta^2 n_l} \right) \right]^{1/2} \tag{14}$$

where

$$\Phi = \frac{8Q^2}{\Delta T(-\cos\theta)qn_p^2} \tag{15}$$

and

$$\psi = \left(\frac{\eta}{c\rho\sigma} \right)_{T_i} \tag{16}$$

A useful form of equation (14) is obtained by combining with equation (7) and rearranging slightly to obtain

$$t_l = \Phi\psi \left(\frac{1 + \dfrac{t_c}{\delta}}{\delta L^2} \right) \tag{17}$$

14

Equation (14) incorporates all the pertinent quantities associated with the radiator save those involving conductive heat transfer as expressed by equation (9). The subscript T_i appended to the bracket in equation (16) indicates that the values assigned to η, c, ρ, and σ must be those that are appropriate to the radiator internal temperature.

In the case of the header arrangement shown in figure 7 the quantity L, representing both header and panel length, imposes a constraint upon δ. An excessive header length, for example, necessitates high pressure drops. This implies, in turn, high capillary pressures that may exceed that required by equation (1) for a given capillary diameter. A significant connection between header length and possible inertial pressures is discussed in appendix C.

In equation (15) the thermal power of the radiator Q is fixed by the mission and/or system requirements. Radiator temperatures T_s, T_i, and ΔT are selected to assure that the properties of the heat exchange liquid assume values compatible with the radiator requirements; in particular, T_i is selected to produce a low vaporization rate. The radiative heat flux q depends upon the nature of the radiator surface selected, the surface temperature T_s, and the dihedral angle ω, which is determined, in turn, by the number of panels, n_p. The quantity $-\cos\theta$ may be arbitrarily set equal to a value ranging from 1/2 to 1 corresponding to $\theta < 120^O$ to 180°. The parameter Φ is thus a constant that is predetermined by the operating conditions and physical and geometric properties of the radiator.

The parameter ψ, which is a composite fluid property, is useful for rating liquids contemplated for use in the capillary radiator. Liquids having low ψ are preferred because, as evident from equation (14), the result is smaller header lengths L in figures 7 and 8, and hence less header pressure drop. Note that ψ has the dimensions of a reciprocal heat transfer coefficient. Fluids with lower values of ψ have better heat transfer characteristics.

Parametric analysis procedure. - Once the parameters Φ and ψ have been assigned values, equation (14) may be used to investigate the range of possible practical capillary diameters. An upper limit is imposed on δ through equation (1) by limits on the minimum operating pressure P, that can be attained. A second upper limit is imposed as a consequence of inertial pressures that result from vehicle accelerations as is explained in appendix C. A third upper limit on δ is imposed by adoption of the Reynolds criterion as follows.

The applicability of the Hagen-Poisseuille equation used in obtaining equation (14) depends on the critical Reynolds number for capillary channels. According to reference 9, experiments have indicated that Darcy's Law and, consequently, the Hagen-Poisseuille equation applies to capillary channels for Reynolds numbers less than roughly 75. This criterion is not well established, and may be several orders lower for capillary channels formed in some types of porous media. Herein the critical Reynolds number is taken as 100; that is,

$$\text{Re} = \frac{v\delta\rho}{\eta} < 100 \tag{18}$$

Combining with equation (13) and substituting P from equation (1) yields

$$\text{Re} = \frac{\rho\sigma(-\cos\theta)}{16\,\eta^2}\left(\frac{\delta^2}{w}\right) < 100 \tag{19}$$

The minimum value of δ is determined by considering the effects of reducing δ upon thermal conduction and radiator weight. Examination of equation (17) reveals that as δ decreases t_l increases for fixed values of Φ, ψ, and t_c/δ. Hence, as is evident from equations (6) and (7), decreasing δ results in increasing t_r. An increase in t_r is necessarily accompanied by a corresponding increase in the internal temperature T_i and a lesser increase in the surface temperature T_s (see eqs. (5) and (9)). However, T_i cannot be increased indefinitely, for the internal temperature must be in a range that does not result in excessive vapor pressure nor extremely low surface tension in the radiator fluid. Hence, a lower bound on δ is set by the overall panel thickness and thermal conduction.

Radiator specific weight also influences the selection of a minimum δ. Note that partitioning material must be added for each diminution of δ; that is, smaller capillaries entail higher containment weight. The consequence of reducing δ is an increase in n_l and t_l (eq. (17)) and a corresponding increase in radiator specific weight with respect to generated power w. This is apparent from examination of equations (21) and (22) in the next paragraph.

An expression for specific weight is obtained by referring to figures 8 and 9 and taking into consideration both the weights of the radiator panels and contained liquid:

$$w = w_c + w_l \tag{20}$$

where

$$w_c = \frac{(1-e)}{e}\,\frac{\rho_c}{2q}\left\{ \frac{\sqrt{\Phi\psi}}{L}\left[\frac{(n_l - 1)\left(1 + \dfrac{t_c}{\delta}\right) + n_l}{\sqrt{n_l}\,\sqrt{1 + \dfrac{t_c}{\delta}}} \right]\left(\frac{t_c}{\delta}\right) + 2t_p \right\} \tag{21}$$

and

16

$$w_l = \frac{(1-e)}{e} \frac{\rho}{2q} \left(\frac{\sqrt{\Phi\psi}}{L} \sqrt{\frac{n_l}{1 + \frac{t_c}{\delta}}} \right) \tag{22}$$

In equation (21) the material densities of the surface plates and capillary partitions represented by thicknesses t_p and t_c, respectively, are assumed equal. Equation (21) is obtained by using the approximate form of equation (8), given that $n_c \gg 1$.

As δ assumes smaller values, either t_c may be constant or the ratio (t_c/δ) may be constant. In each case, all the other quantities in equations (21) and (22) being fixed, both w_c and w_l increase with $n_l\delta$ (=t_l) which, in turn, increases with decreasing δ as stated previously (see eqs. (7) and (17)).

The selection of heat exchange liquid, mean radiator temperature, and other quantities may be predicated on the margin between the minimum and maximum δ. The coincidence or overlap of maximum and minimum values of δ would indicate impracticability under the conditions selected. Because of the monotonic logarithmic functions involved, as in equation (14), the maxima and minima referred to previously are not analytical bounds, but are dependent upon the relative limits assigned to factors such as specific weight, pressure, structure dimensions, and so forth. In general, it is desirable to make δ as small as possible consistent with the limitations mentioned before.

Liquid Loss Considerations

Meteoroid impacts on a capillary radiator panel will result in pressure pulses and punctures. There is insufficient relevant information concerning the intensity and transmittal of pulse pressures in liquid-filled capillary media for estimating liquid escape caused by impact pressures. However, liquid loss by displacement or temporary efflux preceding stabilization of the meniscus, and vaporization can be estimated by considering the frequency and geometry of punctures. Equations for computing the decrement of radiator surface and flow channel areas and liquid loss by displacement and vaporization are presented in this section in correspondence with the radiator configuration described in the section Identification of conditional parameters.

Meteoroid environment. - To determine the effects of the meteoroid environment, it is necessary to select a meteoroid "mass-frequency" distribution relation that best represents the situation during the mission. Mass-frequency distribution data lie in two general categories, one applying to near-Earth and the other to "deep space" or interplanetary regions. Accurate data for deep space are scarce, and curves representing

frequency distributions in the vicinity of the Earth disagree somewhat. However, an analytical expression needs to be adopted in order to estimate the probable rate of meteoroid encounter and extent of damage that may result. A widely accepted meteoroid mass-frequency curve is that of reference 10 known as the Whipple-1961 curve. Although a later revision, Whipple-1963 (ref. 11), indicates a slightly lower meteoroid mass frequency, the earlier version as expressed in the following equation is adopted here:

$$F = 1.246 \times 10^{-15} \, m^{-1.1} \tag{23}$$

Equation (23) represents the cumulate frequency of all meteoroids having a mass equal to and greater than m.

An expression for the total mass encountered by a unit area per unit time for the mass range m_1 to m_2 is obtained as follows: Let dF_m be the total mass flux in the range dm about m. Then.

$$dF_m = F \, dm \tag{24}$$

Integrating between limits m_1 and m_2 yields

$$F_m = \int_{m_1}^{m_2} F \, dm, \qquad m_2 > m_1 \tag{25}$$

Equation (25) implies that particles with masses less than m_1 are inconsequential while those with masses greater than m_2 are too infrequent to be considered in lieu of the radiator area and duration of the mission contemplated.

It should be noted that the aforementioned differs from the approach usually followed in determining anticipated meteoroid encounters (e.g., ref. 1). Conventionally, a Poisson distribution is assumed in order to arrive at an expression for the probability of a vulnerable component being hit by a mass greater than m. Herein it is assumed that the number of encounters for any mass range equals the time-area average of the integrated flux F, that is, a probability factor of one is assumed. This approach places a greater burden on the capillary radiator concept. The survivability of the capillary radiator, unlike the fin-tube radiator, is not rated in terms of the probability of a puncture and consequent total disablement of a vital component. For a puncture in a capillary panel is not equivalent to total loss of that component.

Puncture criteria and loss equations. - All "complete" punctures are idealized as cylindrical holes passing through the radiator panel (fig. 10). A puncture of one surface

18
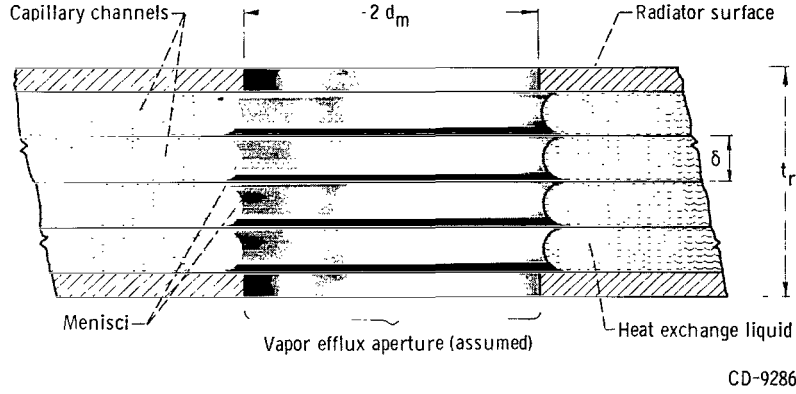
Figure 10. – Cross section of idealized circular meteoroid puncture site.

plate on either side of a panel is considered a complete puncture. Partial penetrations of a surface plate are ignored because the previous criterion for complete punctures is deemed broad enough to include all significant penetrations. Because of the results of the experiments mentioned in appendix D, the diameter of the hole is considered to be invariably twice the "diameter" of the impinging meteoroid irrespective of its shape, mass, or velocity. The meteoroid is assumed spherical, and its diameter d_m is therefore determined by its mass and density; that is,

$$d_m = \left(\frac{6m}{\pi \rho_m}\right)^{1/3} \tag{26}$$

and the radiator area decrement for each puncture is

$$a = 2\pi d_m^2 \tag{27}$$

The differential fractional surface area decrement per unit time dA_s, resulting from puncture by masses in the range dm about m, is

$$dA_s = F\left(\frac{a}{m}\right) dm \tag{28}$$

Using equations (26) and (27) to solve for a as a function of m, substituting for a, and F from equation (23) in equation (28), and integrating yield

$$A_s = (-)3.637 \times 10^{-14} \rho_m^{-2/3} m^{-1/3} \Big|_{m_1}^{m_2} \tag{29}$$

(The exponent of m in eq. (23) is equated to 1 for simplicity.) The fraction of radiator surface area lost during the mission is

$$A_{\tau S} = \tau A_S \tag{30}$$

where τ is the mission duration.

With each puncture the flow channel area diminishes. Because the capillary channels are interconnected, the flow is "two-dimensional"; therefore, the fractional loss of hydraulic area $A_{\tau h}$ is directly proportional to half the fractional loss of radiator area $A_{\tau S}$ if a random puncture pattern exists. The factor one-half appears because A_S in equation (30) represents the two surfaces between which the capillary medium is included.

Similarly, equation (30) also provides an estimate of the fraction of liquid lost by displacement when a puncture occurs. If the diameter of the slug of displaced liquid equals the puncture diameter, then $D_{\tau l}$, the fractional liquid inventory loss by displacement, is given by the following equation:

$$D_{\tau l} = \frac{A_{\tau S}}{2x} \tag{31}$$

In equation (31), x is the factor by which the liquid content of the entire radiator system exceeds the content of the panels.

In figure 10, the area of the hole in the radiator surface and not the exposed liquid area is arbitrarily considered the "effective" area for evaporation. The actual "effective" area depends partially on t_r and the depth-to-diameter ratio of the liquid interface. However, the approach used fixes the area for efflux even if the interface has retracted into the capillary channels. Accordingly, the vapor efflux area for a puncture is permanently established by equation (27). The increment in vapor efflux area caused by masses in the range dm about m equals dA_S (eq. (28)). Assuming a linear increase in the vapor efflux area with time, the average area for vaporization accrued during the mission is

$$A_{\tau l} = \frac{1}{2} n_p LW A_{\tau S} = \frac{QA_{\tau S}}{4q} \tag{32}$$

The rate of evaporation is given by Langmuir's equation (ref. 12) as

$$G = 5.833 \times 10^{-1} P_{mm} \sqrt{\frac{M_g}{T_i}} \tag{33}$$

20

The initial weight of liquid in the radiator, headers, and reservoir is, approximately,

$$I_l = \frac{Q \rho x}{2q} \left(\frac{\delta n_l}{1 + \frac{t_c}{\delta}} \right) \tag{34}$$

The fraction of liquid inventory lost during the mission is

$$I_{\tau l} = \frac{A_{\tau l} G \tau}{I_l} \tag{35}$$

or, substituting from equations (14), (32), (33), and (34),

$$I_{\tau l} = (-)1.0605 \times 10^{-14} \left(\frac{\tau^2 L^2 \delta}{x \Phi T_i^{1/2}} \right) \left(\frac{M_g^{1/2} P_{mm}}{\rho \psi} \right) \left(\rho_m^{-2/3} m^{-1/3} \right) \Big|_{m_1}^{m_2} \tag{36}$$

Note that equation (36) provides a criterion for selecting the heat exchange liquid and radiator temperatures, T_i and also T_s, if $I_{\tau l}$ is preselected.

A further consideration is the relation between the surface plate thickness t_p and the depth to which an impinging meteoroid penetrates the surface plate. The relation depends on the ratio between depth of penetration p and meteoroid diameter d_m, that is, p/d_m. If p/d_m, the meteoroid velocity, mass m, and density ρ_m are specified, it is then possible to estimate the surface plate thickness in which only partial penetrations are likely to occur for meteoroid masses less than a given value. A suitable criterion for selecting t_p should require that for masses less than a minimum value, for example m_1, the effect is equivalent to no penetration at all. Surface plates thinner than this would result in higher rates of liquid exposure because of the higher frequencies of encounter with smaller masses predicted by equations that describe the meteoroid environment (e.g., eq. (23)). Therefore, the selection of t_p depends on the allowable penetration threshold on one hand and its effect on the radiator weight on the other (see eq. (21)).

Establishment of the criterion for t_p mentioned previously is difficult because p and hence p/d_m varies with the meteoroid mass and velocity and because meteoroid densities and shapes vary widely (ref. 13). However, the following approach can be

used: set t_p equal to p and assume a value for p/d_m corresponding to the mean probable velocity. Consequently, p and hence t_p may be regarded as a function of the meteoroid mass through equation (26). Using equations (30) and (36), t_p (=p) may be related through m to the fractional area and liquid inventory losses. Selection of the surface plate thickness will be based on that value of t_p for which the maximum acceptable area or liquid loss occurs.

DISCUSSION OF APPLICATIONS AND PROBLEMS

Illustrative Mission, Configuration, and Conditions

The potential feasibility of the capillary radiator concept may be assessed in terms of the latitude available for selecting such crucial quantities as the capillary diameter, panel dimensions, temperature, hydraulic pressure, and other pertinent dimensions. If a compatible set of the aforementioned quantities exists, it is then necessary to determine whether they lead to acceptably low levels of specific weight, area attrition, and fluid loss. An assessment of potential feasibility in terms of the criteria derived in the previous sections is presented hereinafter in connection with a specific radiator application.

The illustrative example developed in this section concerns a prospective application of the capillary concept which affords a means of comparing the specific weights of capillary and fin-tube radiators. The total radiated heat rejection is arbitrarily set at approximately one-third megawatt. This power level is in the general range contemplated for power system cooling in manned interplanetary vehicles and lunar base powerplants (refs. 14 and 15). Smaller versions of capillary radiators may have applicability to subsystem or component cooling in space vehicles. Examination of equations (14), (15), (21), and (22) will show that for lower power levels the vulnerable area and specific weight are also lower.

The radiator configuration for the following example consists of four orthogonal panels joined to a common header as illustrated in figure 7 (p. 11). Fluid flow within the panels is perpendicular to the header axis as illustrated in figure 8 (p. 12). The capillary substructure is the same as that described previously and illustrated in figure 9 (p. 12).

The following conditions are prescribed:

Duration of mission, τ, sec (days) . . . . 8.64×10^7 (1000)
Power cycle efficiency, e 0.333
Radiator power (rejected heat), Q, W . . . . 0.3×10^6
Radiator surface temperature, T_s, ^{O}K 589
Internal fluid temperature, T_i, ^{O}K 655
Radiator power flux, q, W/m^2 . . . . 4.3×10^3
Heat exchange fluid . . . . Liquid lithium
Material of construction . . . . Titanium

Radiator power rejection is based on a cycle efficiency of 33 percent. To evaluate equation (15), the radiator inlet to outlet temperature difference ΔT is 55.5^O K, and for simplicity it is assumed that all heat is radiated to space at a uniform radiator surface temperature T_s of 589° K. The temperature level of the radiator is arbitrarily selected to yield a low vaporization rate at puncture sites. The heat flux of 4.3×10^3 watts per square meter is based on a radiator surface emissivity ϵ of approximately 0.9 and a configuration factor f_ω of 0.8 (see appendix B). The value of θ in equation (15) is taken as 120 degrees so that $-\cos \theta = 1/2 \leq 1$, the pressure drop criterion cited in the section System interaction factors.

Lithium is selected as the heat transfer liquid primarily because of its low vapor pressure in the temperature range contemplated in the example. Titanium is selected as the containment material because of its compatibility with lithium and its low density. However, neither the fluid nor containment material need be specified. The crucial properties such as density, vapor pressure, and the quantity ψ can be independently specified or treated parametrically. Further analysis might then point to suitable substances.

By selecting the particular radiator configuration, materials, and conditions mentioned previously, it is possible to concentrate upon three factors that are significant in evaluating the capillary radiator's feasibility: capillary diameter, radiator surface attrition, and liquid loss.

Bounds on capillary dimension. - The selection of the capillary diameter is based on equation (1) in this case and evaluated in accordance with the discussion in the section Parametric analysis procedure. Substitution of the conditional values for Φ and ψ in equation (14) yields

$$L = 1.408 \times 10^{-2} \sqrt{\frac{1 + \dfrac{t_c}{\delta}}{\delta^2 n_l}} \tag{37}$$

A plot of L against δ appears in figure 11 where t_c/δ is set equal to 10^{-1} and n_l assumes the values 1, 2, 4, 9, 25, and 81. In this example ψ and σ are assigned values corresponding to $T_i = 655^O$ K for lithium to obtain the expression for L in equation (37).

According to the discussion in the section Parametric analysis procedure, upper bounds on δ are imposed by the Reynolds number, hydraulic pressure requirements, and inertial forces. In the present case these factors collectively dictate an upper bound on δ of about 1.5×10^{-3} to 10^{-2} meter. The calculations for this and the following are discussed in appendix E and the results are summarized in table I.
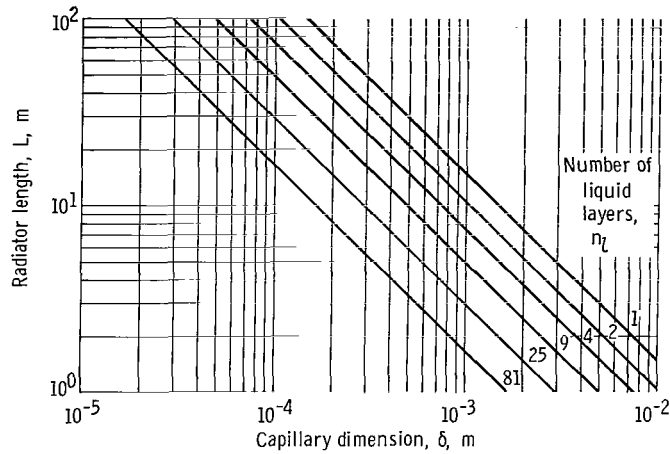
Figure 11. - Covariation of radiator length with capillary dimension and number of capillary layers according to equation (14) for 3×10^5-watt radiator.

TABLE I. - EFFECT OF CAPILLARY

DIMENSION ON SPECIFIC WEIGHT[a]

Capillary diameter, δ, m	Number of layers, n_l	Specific weight of panel alone, w_c, kg/kW	Specific weight with liquid, w, kg/kW
1.5×10^{-3}	1	0.67	0.82
1.1	2	.84	1.1
.73	4	1.0	1.3
.49	9	1.4	1.8
.29	25	2.0	2.8
.16	81	3.2	4.5

[a]Based on equations (21) and (22) and lithium-filled titanium panels with radiator panel and header length $L = 10$ m, radiator surface temperature $T_s = 655^\circ$ K, thickness of surface plate $t_p = 2.54 \times 10^{-4}$ m, $t_c/\delta = 0.1$, power conversion system cycle efficiency $e = 0.333$, and radiator heat flux $q = 4.31 \times 10^3$ W/m^2.

The lower bounds on δ are imposed by heat transfer and specific weight limitations. Given the dimensions and materials of this example, it is found that the more significant lower bound is imposed because of the increase in specific weight w that accompanies the reduction of δ. For instance, δ has a lower bound of roughly $1.5{\times}10^{-4}$ meter if a maximum specific weight of about 5 kilograms per kilowatt is prescribed.

To satisfy the criteria mentioned in the previous paragraphs, δ should lie in the range between $1.6{\times}10^{-4}$ and $1.5{\times}10^{-3}$ meter, approximately. These figures are in the range in δ from $1.5{\times}10^{-4}$ to $1.5{\times}10^{-3}$ meter associated with n_l from 81 to 1, respectively, for the arbitrary selected length of L = 10 meters (see fig. 11).

In the case presented herein it is inferred that the capillary radiator concept is feasible in terms of the heat transfer and fluid dynamic factors corresponding to the bounds on δ. It is noteworthy that the specific weights of a 1/3-megawatt capillary radiator having between 1 and 81 liquid layers are in the same range as those quoted in reference 4 and summarized in table II for a 1/2-megawatt conventional fin-tube radiator. The basis of comparison in this instance is solely the specific weight of the radiator panels exclusive of headers, pumps, and other appurtenances. Note that the specific weights in table II are the minimum values quoted in reference 4 for each material.

Surface area and liquid losses. - Rough estimates of radiator surface area attrition and liquid loss may be made by means of equations (30), (31), and (36). Using the con-

TABLE II. - MINIMUM SPECIFIC WEIGHT FOR

1/2-MEGAWATT FIN-TUBE RADIATOR[a]

Armor materials for tube protection	Specific weight, kg/kW (b)
Columbium alloy (Cb-1Zr)	5
Nickel alloy (Inconel 718)	3.7
Cobalt alloy (L-605)	3.6
Steel (SS 316)	3.3
Molybdenum alloy (TZM)	2.8
Vanadium	2.6
Graphite[c]	1.3
Beryllium[c]	1.0

[a]From ref. 4, specific weights of empty tubes.

[b]Minimum specific weight occurs for all materials at radiator temperatures between 920° and 1030° K in fin-tube radiator.

[c]Includes thin-walled inner liner tube of columbium alloy (Cb-1Zr).

Meteoroid mass, m_1, kg	Surface plate thickness, t_p,[b] m	Fractional radiator area loss, A_{TS} or D_{Tl}[c]	Fractional liquid inventory loss, I_{Tl}[d]
10^{-4}	2.5×10^{-1}	1.7×10^{-7}	0.7×10^{-6}
10^{-6}	2.5×10^{-2}	3.0×10^{-6}	1.4×10^{-5}
10^{-9}	2.5×10^{-3}	3.1×10^{-5}	1.5×10^{-4}
10^{-12}	2.5×10^{-4}	3.1×10^{-4}	1.5×10^{-3}
10^{-15}	2.5×10^{-5}	3.1×10^{-3}	1.5×10^{-2}
10^{-18}	2.5×10^{-6}	3.1×10^{-2}	1.5×10^{-1}

[a]Estimates based on eqs. (26), (30), and (36)
for 1000-day mission.
[b]t_p equated to p (a function of m_1).
[c]Multiply by $\frac{1}{4}$ to obtain fraction of liquid lost
by displacement D_{Tl}.
[d]Based on characteristic capillary dimension
$\delta = 1.5 \times 10^{-3}$ m.

ditions given at the beginning of this section, it was found in appendix E that a 1000-day mission should entail acceptably small losses of area and heat exchange liquid. As indicated in table III, for example, with the surface plate thickness $t_p = 2.5 \times 10^{-4}$ meter, the estimated surface area attrition is 0.03 percent, and liquid loss by evaporation is 0.2 percent, approximately.

Also note that the previous liquid loss figures support the radiator temperature range selected, that is, 589° to 655° K. In fact, for lithium any temperature from approximately 589° to 868° K results in a low loss rate since the corresponding values of G, σ, and ψ do not change significantly for this temperature range. An increase in the radiator temperature permits a corresponding increase in q, the radiative flux, and a corresponding expansion of the bounds of δ and associated quantities through equations (14) and (15).

The figures quoted for the bounds on δ and for area and liquid losses indicate feasibility at least under the selected conditions described in this example. The example given also indicates that a capillary radiator is potentially competitive with conventional radiators up to and including the megawatt range.

Problem Areas and Prospective Advantages

A definitive assessment of the feasibility and applicability of the capillary radiator concept must be deferred until the experimental verification of certain crucial phenomena has been accomplished. For example, studies of surface tension and vaporization phenomena in capillary media under high temperature, vacuum conditions are needed to support the values assumed herein. For the same reason, specific and accurate information concerning heat transfer, flow, pressure drop, and temperature distribution in porous media of the types suitable for a capillary radiator is needed. Indeed, the production and fabrication of capillary media that can be effectively incorporated into radiator panels are potentially problematic and require developmental effort.

Some aspects of capillary retention under dynamic flow conditions may require scale model studies for further verification of workability. Also, the possible presence and effects of noncondensable gases on capillary retention should be assessed.

A vital area for further inquiry concerns the effects of meteoroid impacts on liquid-filled capillary media. Experimental information is needed to define the characteristics of impact damage in various capillary structures and to determine the effects of intense pressure pulses on the structures and contained fluid. For example, under certain conditions, highly localized, short duration pressure pulses may be exerted which are of the order of billions of newtons per square meter and last roughly 100 microseconds (ref. 16). The evolution of suitable capillary substructures and modes of fabrication will be necessary to circumvent the possible deleterious effects of impact shocks. The aforementioned experiments and developmental efforts should be tailored for testing under conditions duplicating the zero- or low-gravity environment of an actual space application.

Because the heat exchange liquid should have high surface tension and low vapor pressure, the choice of fluids for high temperature operation may be somewhat restricted. For example, only liquid metals appear to possess suitable properties in the high temperature, kilowatt to megawatt range. In this case, the problem of containment material compatibility also arises. An investigation of corrosion and dissolution phenomena in porous media would be required in order to establish evidence of long term integrity of capillary media. In addition, means of inducing wetting where needed while inhibiting unwanted spreading of the liquid over the radiator surface should be developed to optimize the surface tension phenomena upon which the retention concept is predicated.

Incorporation of the capillary radiator concept into a viable system poses a number of engineering problems. The evolution and development of suitable modes of pumping, fluid distribution; and pressure, temperature, and inventory control may be problematic. These factors might dictate the ultimate forms, applications, and limitations of the capillary radiator concept.

Among the potential advantages is the possible reduction of radiator weight with respect to power. Excluding the pump, headers, and supports structure, the radiator specific weight might be reduced substantially below values usually quoted for armored fin-tube radiators. Another potential advantage is afforded by the low operating temperature which may be as much as 650° K lower than that contemplated for an equivalent fin-tube radiator (refs. 1 to 3). The temperature advantage accrues because a considerably larger, prime heat radiating surface area is possible. This, in turn, is a consequence of the fact that it is necessary neither to confine the heat exchange liquid in a small number of widely spaced flow channels nor to depend crucially upon conductive heat transfer to the radiating surface. The low radiator temperature may be utilized either to increase cycle efficiency or to lower the overall temperature level of the power system. Also the overall size or area of the radiator is not as critical as in a conventional fin-tube radiator because the area vulnerable to punctures need not be reduced to avoid punctures.

In addition to the potential advantages mentioned previously, it may be possible to eliminate redundant radiator segments that are contemplated for fin-tube radiators (ref. 6). Also, the thin panels or fins in a capillary radiator may offer more configurational flexibility for launch folding and deployment.

It should be noted that prospective applications of this concept are not limited to heat rejection in large powerplants, but may include the cooling of smaller components and subsystems.

CONCLUDING REMARKS

The capillary radiator concept described herein is suggested for use in space heat rejection systems. If the requisite conditions for capillary retention of liquid described herein are met, it appears possible to construct capillary radiators that satisfactorily survive the effects of meteoroid impact damage.

Although liquid retention at puncture sites by surface tension effects is theoretically possible by using appropriate capillary media, more studies are needed to confirm the viability of a liquid-filled capillary radiator under the full range of conditions prevailing in an actual application. Such effort seems merited because a capillary radiator may offer advantages that are suitable to space power systems. The chief potential relative advantages are (1) lower system temperature or higher theoretical powerplant cycle efficiency, (2) adaptability to various power systems and configurational flexibility, (3) lower panel weight with respect to electric power produced, and (4) less restriction on the radiator size.

Before the potentialities of the capillary concept can be realized, however, a number of technical and developmental problems will have to be resolved. In particular, the effects of hypervelocity impacts on liquid-filled capillary media should be investigated and means for producing suitable capillary structures should be developed.

Lewis Research Center,
   National Aeronautics and Space Administration,
      Cleveland, Ohio, September 25, 1967,
         120-27-02-08-22.

APPENDIX A

SYMBOLS

A_s fractional area loss per unit time (eq. (29)), $\sec^{-1}$

$A_{\tau h}$ fraction of hydraulic cross section lost

$A_{\tau l}$ mean equivalent liquid area exposed (eq. (32)), m^2

$A_{\tau s}$ fraction of radiator area lost during mission (eq. (30))

a radiator area decrement, m

c specific heat of radiator liquid, $J/(kg)(K)$

$D_{\tau l}$ fraction of liquid lost by displacement (eq. (31))

d puncture diameter, m

d_m meteoroid diameter, m

e power conversion system cycle efficiency

F cumulate meteoroid frequency, $(m^{-2})(\sec^{-1})$

F_m integrated mass flux (eq. (25)), $kg/(m^2)(\sec)$

f_ω configuration factor (eq. (38))

G evaporation rate, $kg/(m^2)(\sec)$

g acceleration, $m/\sec^2$

g_o acceleration due to gravity, $9.80\ m/\sec^2$

I_l liquid inventory, kg

$I_{\tau l}$ fraction of inventory lost (eq. (36))

i_π quantity proportional to total heat flux when $\omega = 180^o$

i_ω quantity proportional to heat flux for dihedral angle ω (eq. (39))

k thermal conductivity, $W/(cm)(K)$

L radiator panel and header length, m

dl differential length of meniscus (fig. 4), m

M mass flow rate per panel, kg/sec

M_g gram molecular weight, g

m meteoroid mass, kg

m_1 minimum mass (integration limit), kg

m_2 maximum mass (integration limit), kg

n_c number of capillary channels per layer

n_l number of liquid layers

n_p number of radiator panels

P radiator inlet pressure, N/m^2

ΔP radiator pressure drop, N/m^2

P_g inertial pressure (eq. (43)), N/m^2

P_{mm} vapor pressure at $\frac{1}{2}(T_i + T_s)$, mm Hg

p depth of penetration, m

Q thermal power rejected by radiator, W

q radiator heat flux, W/m^2

Re	capillary Reynolds number (eq. (19))	δ_g	equilibrium capillary dimension for inertial pressure (eq. (44)), m
ΔT	inlet to outlet temperature difference in radiator, K	δ'	local capillary dimension (fig. 4), m
T_i	maximum radiator internal temperature, K	δ'_e	equilibrium capillary dimension for parallel plate capillary (eq. (2)), m
T_s	radiator surface temperature, K	δ''	arc length of differential meniscus (fig. 4), m
t_c	thickness of capillary or layer partition, m	ϵ	thermal emittance
t_l	total fluid cross section thickness, m	η	viscosity, $(N)(sec)/m^2$
t_p	thickness of surface plate, m	θ	$\theta_c \le \theta \le 180^o$, angle with respect to container surface at edge, deg (fig. 2(b))
t_r	overall thickness of radiator panel, m		
v	liquid velocity in radiator panel, m/sec	θ'	liquid surface angle of contact with respect to contiguous element of liquid, deg
W	width of radiator panel, m		
w	total specific weight of radiator panel (eq. (20)), kg/W	θ_c	equilibrium contact angle, deg
w_c	specific weight of capillary panel (eq. (21)), kg/W	ρ	liquid density, kg/m^3
		ρ_c	channel material density, kg/m^3
w_l	specific weight of heat exchange fluid (eq. (22)), kg/W	ρ_m	meteoroid density, kg/m^3
x	inventory factor $(x > 1)$ (eq. (31))	σ	surface tension, N/M
y	variable length (eq. (40)), arbitrary units	σ_B	Stefan-Boltzmann constant, $5.6697 \times 10^{-8} \ W/(m^2)(K^4)$
β	variable angle (eq. (39))	τ	mission duration, sec
δ	characteristic capillary dimension, m	Φ	parametric constant (eq. (15))
		φ	variable angle (eq. (39))
δ_e	equilibrium capillary dimension for tubular capillary (eq. (1)), m	ψ	fluid parameter (eq. (16))
		ω	dihedral angle between radiator panels, deg

APPENDIX B

CONFIGURATION FACTOR

In a radiator consisting of panels that are arranged to form dihedral angles as in the case illustrated in figure 7, a portion of the radiated heat is intercepted by adjacent panels. The amount that is intercepted depends upon the dihedral angle ω. The fraction of the total heat radiated that escapes to space (regarded as a perfect heat sink) is a function of the temperature, emissivity, reflectance, and absorptivity integrated over the surface of the panel. For simplicity, the configuration factor derived hereinafter is based upon the following conditions:

(1) The radiation intensity in any direction varies as the cosine of the angle to the normal of the surface, Lambert's cosine principle.

(2) Temperature and emissivity are constant over the radiator surface.

(3) The panels are infinitely long and equal in width.

(4) Reflected radiation is nil, and all intercepted reemitted radiation is nil.

The configuration factor f_ω is defined by equation (38)

$$f_\omega = \frac{i_\omega}{i_\pi} \tag{38}$$

where i_ω is proportional to the total heat flux emitted by a panel that forms a dihedral angle ω with respect to an identical adjoining panel and i_π is proportional to the total heat flux when ω equals 180° (see fig. 12). The defining equation for i_ω is

$$i_\omega = \int_0^1 \int_0^{\pi/2} \int_{\beta_1}^{\pi} \sin\beta \, dy \, d\varphi \, d\beta \tag{39}$$

where

$$\beta_1 = \arctan\left(\frac{\sin\omega \, \cos\varphi}{y - \cos\omega}\right) \tag{40}$$

Because the width of each panel W is identical, the limit on y may be set equal to unity, as in equation (39).
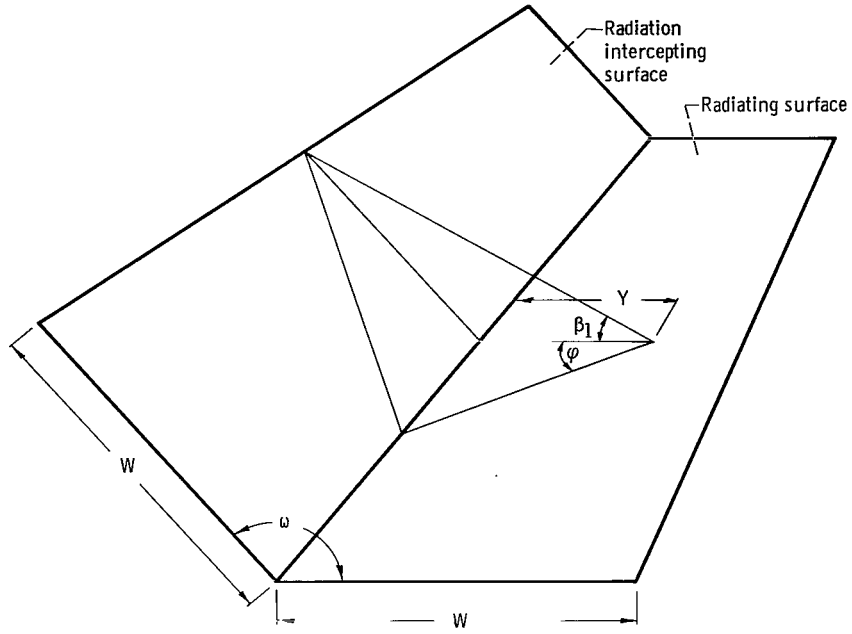
Figure 12. – Diagram of radiator panels.

CD-9287

Integration of equation (39) and simplification yield

$$i_\omega = \frac{\pi}{2} + 2 \sin \frac{\omega}{2} \; E\left(\frac{\pi}{2} \middle| \cos^2 \frac{\omega}{2}\right) \; - \; E\left(\frac{\pi}{2} \middle| \sin^2 \omega\right) \tag{41}$$

where

$$E\left(\frac{\pi}{2} \middle| \cos^2 \frac{\omega}{2}\right) = \int_0^{\pi/2} \sqrt{1 - \cos^2 \frac{\omega}{2} \sin^2 \varphi} \; d\varphi \tag{42a}$$

and

$$E\left(\frac{\pi}{2} \middle| \sin^2 \omega\right) = \int_0^{\pi/2} \sqrt{1 - \sin^2 \omega \sin^2 \varphi} \; d\varphi \tag{42b}$$

Equations (42a) and (42b) are elliptical integrals of the second kind which, when evaluated for $\omega = 90^\circ$, 120°, and 180°, yield the values of f_ω shown in table IV.

The values thus obtained for f_ω are less than those that are obtained by including radiation reflected from the adjacent panel. The expression derived for f_ω is, however,

TABLE IV. - CONFIGURATION FACTORS

Dihedral angle between radiator panels, ω, deg	Quantity proportional to radiation intensity (eq. (39)), i_ω	Configuration factor (eq. (38)), f_ω
$\pi/2$	2.484	0.793
$2\pi/3$	2.902	.925
π	3.141	1.0

considered appropriate in the present case because it represents the lower bound for the panel arrangements presented.

APPENDIX C

INERTIAL PRESSURES

In a capillary radiator inertial pressure variations of long duration or high intensity can have undesirable consequences. If the radiator is designed to operate at very low pressures, then its incorporation into a space vehicle that is subjected to high maneuvering accelerations may be inadvisable because of possible overpressures. Excessive pressure at puncture sites would inevitably result in liquid escape. In general, interplanetary missions are expected to entail rather low accelerations (ref. 17). Anticipated accelerations need to be considered in selecting a capillary dimension and header length to assure that pressure due to acceleration can be supported by surface tension forces.

The greatest potential contribution to the inertial pressure is made by the longest liquid-filled component which is the header with length L in the radiator model described in the section Heat Transfer and Fluid Dynamic Considerations. The maximum inertial pressure P_g arising when the vehicle acceleration g occurs in the direction of the header axis is

$$P_g = \rho L g_0 \left(\frac{g}{g_0}\right) \tag{43}$$

where g_0 is acceleration of gravity at the Earth's surface. Given the acceleration schedule of the vehicle during flight, comparison with the following equation:

$$\delta \leq \delta_g = \frac{4\sigma(-\cos\theta)}{\rho L g_0} \left(\frac{g_0}{g}\right), \qquad P_g = P \tag{44}$$

reveals whether the capillary diameter based on pump pressure through equation (1) is realistic. Or, combining equations (43) and (44) results in an expression for g in terms of the ratio P_g/P, that is,

$$\frac{g}{g_0} = \frac{4\sigma(-\cos\theta)}{\delta \rho L g_0} \left(\frac{P_g}{P}\right), \qquad P_g \neq P \tag{45}$$

and stipulating a maximum tolerable value for P_g/P, for example 0.1, yields a limit for inflight accelerations. Also, as is evident from equation (44), assignment of values to g/g_0 and P_g/P imposes restrictions upon the quantity $\delta_g \rho L$. Obviously, the selection of a low density liquid is desirable not only to reduce radiator specific weight but to increase the limit on acceleration.

APPENDIX D

PUNCTURES IN TYPICAL CAPILLARY STRUCTURES

Meteoroid damage to prospective capillary media should be assessed by examining punctures in representative liquid-filled radiator segments. The type of information needed in order to make this assessment is presently unavailable.

The experiments described hereinafter indicate the damage that can be expected in an unfilled capillary medium of the type that may be suitable for a capillary radiator. These were low velocity projectile firings that yielded tentative information concerning the relationship between hole size, projectile diameter, and velocity.

A typical result was obtained by firing a projectile at a corrugated steel target which represented a prospective capillary radiator panel segment. Two corrugated stainless-steel plates about 0.038 centimeter thick were spot-welded together with their corrugations crossing at right angles. The projectile was a 0.556-centimeter stainless-steel


C-65-3403
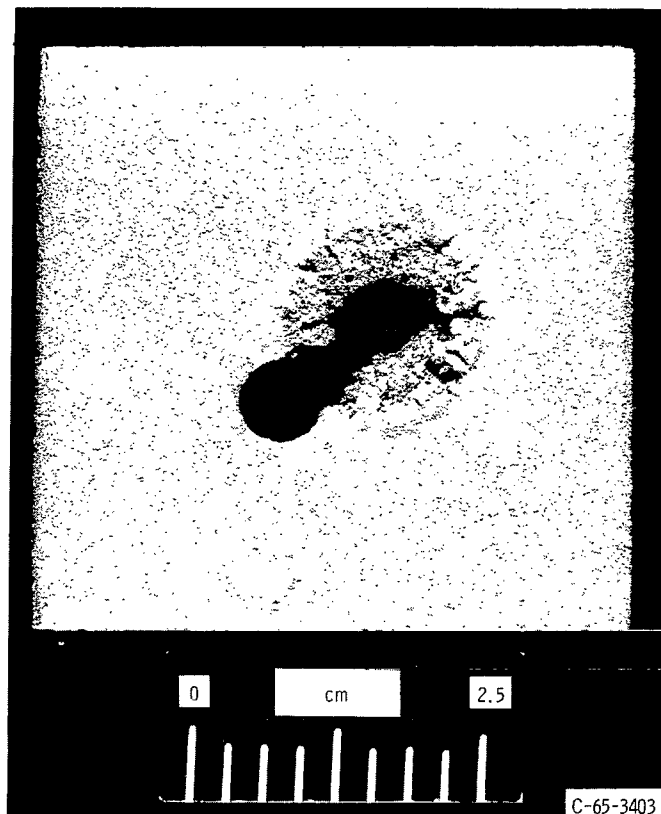
Figure 13. - Simulated meteoroid penetration of foam metal target representing capillary radiator segment.

sphere traveling with a velocity of approximately 1524 meters per second. Examination of the target revealed a clean hole on the impact side with a diameter slightly larger than the projectile. The ragged hole on the reverse side was roughly twice the diameter of the projectile.

The result of firing a 0.556-centimeter-diameter stainless-steel ball into a porous nickel target is shown in figure 13. The target was 0.653 centimeter thick and its density was about 20 percent of the density of solid pure nickel. Two adjacent impacts were
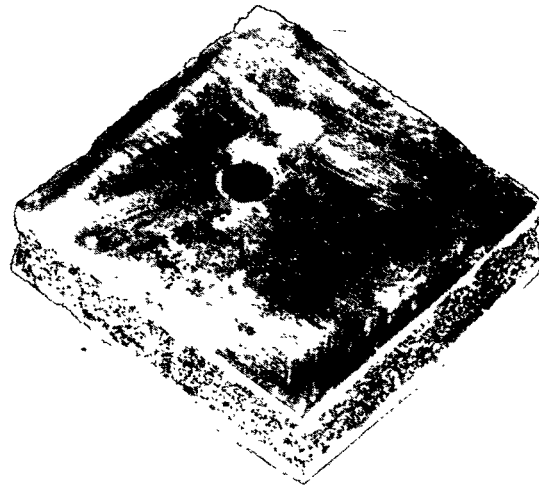
C-66-384

(a) Projectile entrance side of target.
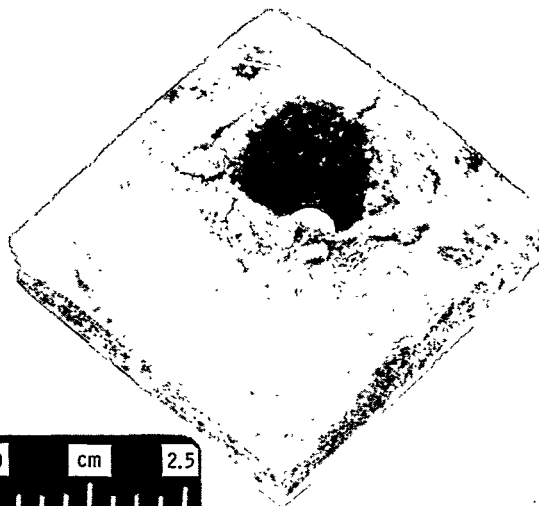
C-66-385

(b) Projectile exit side of target.

Figure 14. - Simulated meteoroid impact of foam metal target representing capillary radiator segment.

37

made at approximately 1524 meters per second against opposite sides of the target. The ball made a clean circular hole on the side facing the gun in each case. The craters formed on the opposite sides had a ragged, approximately conical shape, and were again roughly twice the projectile diameter.

Another target tested was a monometallic sandwich consisting of three bonded layers of foam nickel. The two outer layers, approximately 0.317 centimeter thick, consisted of 20 percent density nickel. The middle layer, approximately 0.794 centimeter thick, consisted of 7 percent density nickel. The foam nickel sandwich was impacted in the same manner as the aforementioned targets described previously. As seen in figure 14(a), the side facing the gun had a clean circular hole slightly larger than the 0.556 centimeter diameter of the projectile. The opposite side had a bowl-shaped cavity with a diameter of approximately twice the projectile diameter, as seen in figure 14(b).

The hole- to projectile-diameter ratios produced by the low velocity experiments described in the previous paragraphs are not necessarily representative of ratios produced by projectiles with higher velocities. In lieu of pertinent high velocity data, however, a two-to-one ratio was adopted herein in the analysis of meteoroid puncture effects.

APPENDIX E

EVALUATION OF CRITICAL PARAMETERS

The limitations on the capillary diameter and estimates of radiator area attrition and liquid loss are discussed in terms of the hypothetical example and conditions described in the text in the section Illustrative Mission, Configuration, and Conditions.

Limitations on Capillary Dimension

Upper bounds on δ are imposed by the Reynolds number, hydraulic pressure, and inertial forces (see the section Parametric analysis procedure). Evaluation of equation (19) yields a Reynolds number that is below the adopted criterion value of 100 for capillary diameters less than 10^{-2} meter. An upper bound is also imposed by the minimum practical pressure that can be used in the capillary system. The minimum pressure is dictated in part by the return header inlet pressure which is a function of the header dimensions. If a 7.6-centimeter-diameter return header 10 meters long is assumed, then the return header inlet and, hence, radiator inlet pressure should be of the order of 70 newtons per square meter since $\Delta P = 1/2 \, P$. From equation (1) the capillary diameter corresponding to a pressure of 70 newtons per square meter is about 10^{-2} meter. As discussed in appendix C, an upper bound is imposed on δ by inertial forces that arise in a space vehicle. Using equation (44) and assuming that g/g_0 ranges from 10^{-2} to 10^{-3} yields δ_g ranging from 1.5×10^{-3} to 1.5×10^{-2} meter, respectively. An upper bound of $\delta = 1.5 \times 10^{-2}$ meter approximately, corresponds to the low accelerations associated with electrically propelled interplanetary vehicles (ref. 17). The previous conditions therefore collectively dictate an upper bound on δ between 1.5×10^{-3} to 10^{-2} meter.

Given the dimensions and materials of this example, the lower bound imposed by conductive transfer within the panels is considerably less than that imposed by the increase of specific weight that accompanies the reduction of capillary diameter. Table I indicates the increase in specific weight with the decrease in diameter for titanium radiator panels. The second column indicates the number of liquid layers n_l and the first column the associated capillary diameter obtained by solving equation (37) for δ. The specific weights w_c in the third column for panels of titanium are obtained with equation (21) by assuming a surface plate thickness t_p of 2.54×10^{-4} meter and $t_c/\delta = 10^{-1}$. The same value for t_c/δ was assumed in using equation (22) for computing the liquid specific weights to obtain the total specific weight of a lithium-filled panel w in the last column (where $w = w_c + w_l$, eq. (20)).

Note that the figures in table I are estimates of weight with respect to electric power of only the radiating panels and contained liquid and do not include the specific weights of the headers, manifolding, pumps, and support structures associated with the radiator. Note also that the specific weight of the liquid adds significantly to the total specific weight (compare the last two columns). The specific weights quoted in table I would be reduced by a substantial amount in the case of the capillary medium shown in figure 9 if the channel and layer partitions were discontinuous instead of solid.

Upon the basis of the foregoing evaluation, δ has a lower bound of roughly 1.6×10^{-4} meter if a maximum specific weight of about 5 kilograms per kilowatt (electric) is prescribed. Consequently, upon this arbitrary basis and the upper bounds mentioned previously, δ lies in the range from 1.6×10^{-4} to 1.5×10^{-3} meter approximately.

Surface Area Losses and Liquid Inventory Losses

An important factor in estimating liquid and radiator area losses is the surface plate thickness t_p. Using the method suggested in the section Puncture criteria and loss equations, t_p is equated to p thus varying with m_1, the minimum mass for which a complete puncture occurs.

Radiator area attrition and fluid loss for a 1000-day exposure are shown in table III as a function of meteoroid mass. To calculate these quantities, the upper limit m_2 in equations (30) and (36) is set equal to 10 grams. Masses greater than 10 grams are ignored because due to a low rate of encounter, they are unlikely to contribute significantly to area or fluid attrition rates. This is apparent by inspection of the last two columns in table III. There is no need to specify the lower limit m_1 because the assumed radiator surface plate thickness determines those masses producing only partial penetrations which are therefore ignorable according to the criterion adopted in the text. In the first column of table III, the mass range for m_1 from 10 to 10^{-15} gram adequately covers the fields of interest. To calculate values for the remaining columns, the meteoroid density is set to equal 1 gram per cubic centimeter (ref. 20) and the meteoroid diameters are calculated from equation (26). Depths of penetration into the surface plate based on $p/d_m = 20$ (ref. 13) are listed in the second column. Because the surface plate thickness t_p is set equal to p for each value of p appearing in the second column, all masses equal to or greater than each succeeding m_1 produce a complete puncture. The third column lists the fraction of original area lost during a 1000-day mission computed by equation (30). The fraction of original liquid inventory lost by vaporization computed by equation (36), with $x = 2$, is listed in the last column. Liquid loss by displacement is obtained by multiplying 1/4 (i.e., $1/(2x)$) times the figures in the third column of table III. The values in table III are rough estimates based on the assumptions discussed previously.

The selection of the radiator surface plate thickness may be based partly on the figures appearing in table III and partly upon the estimates of depth of corrosive attack. If the depth of corrosive attack during the mission were less than 2.5×10^{-6} meter, then even a minimum surface plate and partition thickness t_p and t_c, respectively, of about 2.5×10^{-5} meter appears practicable. A review of pertinent corrosion data indicates that this assumption is realistic (refs. 18, 19, and 20). However, for plate thicknesses between about 2.5×10^{-3} and 2.5×10^{-4} meter, full penetration by masses ranging down to between 10^{-9} and 10^{-12} kilogram is predicted by table III. A thickness of 2.5×10^{-4} meter results in an area attrition of 0.03 percent and combined fluid loss by evaporation and displacement of 0.2 percent, approximately, according to the estimates presented in the tabulation. These figures support the surface plate thickness used previously to arrive at the specific weights quoted in table I. Note that even if the loss estimates in table III are too low by a factor of 10, the losses of area and fluid would still be relatively small.

Corroborative estimates of depth of penetration in aluminum and steel made by the authors of references 21 and 22, respectively, indicate it is unlikely that meteoroids less than 10^{-6} gram can penetrate plates thicker than 2.5×10^{-4} meter. In view of this and the preceding discussion, it appears that a minimum radiator surface plate thickness of about 2.5×10^{-4} meter is adequate for most candidate materials in order to maintain a low puncture frequency and low liquid loss.

REFERENCES

1. Loeffler, I. J.; Lieblein, Seymour; and Clough, Nestor: Meteoroid Protection for Space Radiators. Power Systems for Space Flight. Vol. 11 of Progress in Astronautics and Aeronautics. Morris Zipkin and Russell N. Edwards, eds., Academic Press, 1963, pp. 551-579.

2. Krebs, Richard P.; Winch, David M.; and Lieblein, Seymour: Analysis of a Megawatt Level Direct Condenser-Radiator. Power Systems for Space Flight. Vol. 11 of Progress in Astronautics and Aeronautics. Morris Zipkin and Russell N. Edwards, eds., Academic Press, 1963, pp. 475-504.

3. Haller, Henry C.; and Lieblein, Seymour: Feasibility Studies of Space Radiators Using Vapor Chamber Fins. Paper presented at the Heat Pipe Conference, AEC, Albuquerque, New Mexico, June 1, 1966.

4. Clough, Nestor; Diedrich, James H.; and Lieblein, Seymour: Results of Hypervelocity Impacts into Space Radiator Materials. Paper presented at the AIAA First Rankine Cycle Space Power Systems Specialists Conference, Cleveland, Oct. 26-28, 1965.

5. Diedrich, James H.; and Lieblein, Seymour: Materials Problems Associated with the Design of Radiators for Space Powerplants. Power Systems for Space Flight. Vol. 11 of Progress in Astronautics and Aeronautics. Morris Zipkin and Russell N. Edwards, eds., Academic Press, 1963, pp. 627-653.

6. English, Robert E.; and Guentert, Donald C.: Segmenting of Radiators for Meteoroid Protection. ARS J. vol. 31, no. 8, Aug. 1961, pp. 1162-1164.

7. Adam, Neil K.: The Physics and Chemistry of Surfaces. Third ed., Oxford University Press, 1941, pp. 192-194.

8. Reynolds, William C.; and Satterlee, Hugh M.: Liquid Propellant Behavior at Low and Zero g. The Dynamic Behavior of Liquids in Moving Containers, H. Norman Abramson, ed. NASA SP-106, 1966, pp. 393, 411-412.

9. Scheidegger, Adrian E.: The Physics of Flow Through Porous Media. University of Toronto Press, 1957, pp. 92-93, 124-125.

10. Whipple, Fred L.: Particulate Contents of Space. Symposium on Medical and Biological Aspects of Energies of Space. Paul A. Campbell, ed., Columbia University Press, 1961, pp. 49-70.

11. Whipple, Fred L.: On Meteoroids and Penetration. Advances in the Astronautical Sciences. Vol. 13. Eric Burgess, ed., Western Periodicals Co., 1963, pp. 590-598.

12. Dushman, Saul (J. M. Lafferty, ed.): Scientific Foundations of Vacuum Technique. Second ed., John Wiley & Sons, Inc., 1962, p. 14.

13. Cosby, William A.; and Lyle, Robert G.: The Meteoroid Environment and Its Effects on Materials and Equipment. NASA SP-78, 1965.

14. Anon.: Systems for Nuclear Axuiliary Power: Report by the Commission - 1964. Rep. No. TID-20103, USAEC, Feb. 1964.

15. Anon.: Systems for Nuclear Auxiliary Power. An Evaluation - January 1964. Rep. No. TID-20079, USAEC, 1964.

16. Stepka, Francis S.; Morse, C. Robert; and Dengler, Robert P.: Investigation of Characteristics of Pressure Waves Generated in Water Filled Tanks Impacted by High-Velocity Projectiles. NASA TN D-3143, 1965.

17. Melbourne, W. G.: Interplanetary Trajectories and Payload Capabilities of Advanced Propulsion Vehicles. Tech. Rep. 32-68, Jet Propulsion Lab., California Inst. Tech., Mar. 31, 1961.

18. Di Stefano, James R.: Corrosion of Refractory Metals by Lithium. Rep. No. ORNL-3551, Oak Ridge National Lab., Mar. 1964.

19. Di Stefano, J. R.; and Hoffman, E. E.: Corrosion Mechanisms in Refractory Metal-Alkali Metal Systems. The Science and Technology of Tungsten, Tantalum, Molybdenum, Niobium and Their Alloys. N. E. Promisel, ed. AGARDograph-82, McMillan Co., 1964, pp. 257-288.

20. Minushkin, Bertram: Determination of the Solution Rate of Metals in Lithium. Rep. No. NDA-44 (Del.), Nuclear Development Corp. of America, Nov. 10, 1958.

21. Whipple, Fred L.: The Meteoritic Risk to Space Vehicles. Vistas in Astronautics. Vol. I. Morton Alperin, Marvin Stern, and Harold Wooster, eds., Pergamon Press, 1958, pp. 115-124.

22. Bjork, R. L.: Meteoroids vs. Space Vehicles. ARS J., vol. 31, no. 6, June 1961, pp. 803-807.